Development/Plasticity/Repair

Transcriptional and Electrophysiological Maturation of Neocortical Fast-Spiking GABAergic Interneurons

Benjamin W. Okaty,* Mark N. Miller,* Ken Sugino, Chris M. Hempel, and Sacha B. Nelson
Department of Biology, Brandeis University, Waltham, Massachusetts 02453

Fast-spiking (FS) interneurons are important elements of neocortical circuitry that constitute the primary source of synaptic inhibition in adult cortex and impart temporal organization on ongoing cortical activity. The highly specialized intrinsic membrane and firing properties that allow cortical FS interneurons to perform these functions are attributable to equally specialized gene expression, which is ultimately coordinated by cell-type-specific transcriptional regulation. Although embryonic transcriptional events govern the initial steps of cell-type specification in most cortical interneurons, including FS cells, the electrophysiological properties that distinguish adult cortical cell types emerge relatively late in postnatal development, and the transcriptional events that drive this maturational process are not known. To address this, we used mouse whole-genome microarrays and whole-cell patch clamp to characterize the transcriptional and electrophysiological maturation of cortical FS interneurons between postnatal day 7 (P7) and P40. We found that the intrinsic and synaptic physiology of FS cells undergoes profound regulation over the first 4 postnatal weeks and that these changes are correlated with primarily monotonic but bidirectional transcriptional regulation of thousands of genes belonging to multiple functional classes. Using our microarray screen as a guide, we discovered that upregulation of two-pore K^+ leak channels between P10 and P25 contributes to one of the major differences between the intrinsic membrane properties of immature and adult FS cells and found a number of other candidate genes that likely confer cell-type specificity on mature FS cells.

Introduction

Cortical GABAergic interneurons can be segregated into distinct subtypes based on their morphology, electrophysiology, synaptic connectivity, and gene expression (Kawaguchi and Kondo, 2002; Markram et al., 2004; Nelson et al., 2006). How these complex phenotypes develop remains an open question. Given that GABAergic interneuron subtypes support diverse cortical circuit functions, such as mediating critical period plasticity (Hensch et al., 1998; Di Cristo et al., 2007; Katagiri et al., 2007), entraining network activity oscillations (Cobb et al., 1995; Bartos et al., 2002, 2007; Doischer et al., 2008), and maintaining the balance of excitation and inhibition (Treiman, 2001; Le Roux et al., 2008; Wang and Kriegstein, 2008), progress toward understanding the mechanisms that promote and maintain interneuron identity is of broad importance.

Mounting evidence suggests that the location and time of birth of prospective interneurons dictates their mature phenotype in part by initiating divergent transcriptional cascades in the embryo (Xu et al., 2004; Butt et al., 2005, 2007; Cobos et al., 2006; Wonders and Anderson, 2006; Flames et al., 2007). Although the full transcriptional networks mediating fate determination and differentiation of cortical interneurons have yet to be resolved, steady progress has been made in identifying a number of the key regulators operating at early stages of development in the embryo, such as *Dlx1/2*, *Nkx2.1*, *Lhx6*, and *Arx* (Sussel et al., 1999; Butt et al., 2008; Xu et al., 2008). However, a detailed description of the postnatal transcriptional and phenotypic maturation of interneuron subtypes is presently lacking. Knowledge at this level is essential to elucidating the function of gene networks operating downstream of early induced transcription factors, particularly because these may directly mediate specific aspects of the mature phenotype. We address this question for one particular interneuron subtype, cortical parvalbumin (PV)-expressing fast-spiking (FS) GABAergic interneurons, for which a genetically labeled mouse line has afforded reliable targeting. We characterized both whole transcriptome expression and the electrophysiology of these cells at a range of postnatal ages and found that FS cells exhibit profound developmental regulation of both gene expression and physiology over the first 4 postnatal weeks. Developmentally regulated genes spanned multiple functional categories but were significantly enriched for ion channels and showed predominantly monotonically increasing or decreasing expression trajectories. Comparing the temporal patterns of gene regulation revealed by our microarray with maturational changes in the intrinsic and synaptic properties of FS cells allowed us to correlate the expression of subsets of genes with the onset of multiple FS cell phenotypes. In particular, we demonstrate that upregulation of two-pore K^+ leak channels

Received Jan. 8, 2009; revised March 17, 2009; accepted April 21, 2009.

This research was supported by grants from National Institute of Mental Health and the Simons Foundation (S.B.N.) and National Institute of Neurological Disorders and Stroke (M.N.M.). We thank Zhe Meng for technical assistance and Josh Huang for providing transgenic mice.

*B.W.O. and M.N.M. contributed equally to this work.

Correspondence should be addressed to Sacha B. Nelson, Biology Department, MS-008, Brandeis University, 415 South Street, Waltham, MA 02453. E-mail: nelson@brandeis.edu.

M. N. Miller's present address: Keck Center for Integrative Neuroscience, Department of Physiology, University of California, San Francisco, San Francisco, CA 94143.

C. M. Hempel's present address: Galenea Corp., Cambridge, MA 02139.

DOI:10.1523/JNEUROSCI.0105-09.2009

 0270-6474/09/297040-13$15.00/0

contributes to the characteristic low input resistance of mature FS cells.

Materials and Methods

Transgenic mice. We used the G42 transgenic mice described by Chattopadhyaya et al. (2004) for all experiments. All procedures were conducted in accordance with National Institutes of Health guidelines for animal use and were approved by the Brandeis University animal use committee. Briefly, G42 mice were engineered by the genomic incorporation of a 200 kb GAD1 bacterial artificial chromosome fused to the enhanced green fluorescent protein (GFP) coding sequence. Because of a combination of promoter and position of integration effects, GFP expression is restricted to a homogenous subset of GABAergic interneurons distinguished in the adult mouse brain by their capacity to fire at high rates (>200 Hz) and by the expression of the calcium binding protein parvalbumin, which emerges between postnatal day 10 (P10) and P15. Before the expression of parvalbumin, developing G42 cells express other cell-type-specific markers (supplemental Fig. S1*a*, available at www.jneurosci.org as supplemental material). Cortical expression of GFP-positive neurons was restricted to layers 2/3, 5, and 6, with occasional expression in layer 4 and no expression in ventral regions of cortex at all studied ages (supplemental Fig. S1*b*, available at www.jneurosci.org as supplemental material). Additionally, G42 biocytin-filled cells prepared after recording at P7, P10, P15, and P25 (see methods below) were all multipolar and lacked an apical dendrite or pyramidal-shaped soma suggestive of excitatory cells. These observations, together with the results of clustering analysis performed on gene expression profiles across multiple cell types (supplemental Fig. S1*c*, available at www.jneurosci.org as supplemental material), suggest that the G42 line is a stable marker of prospective fast-spiking PV-positive cortical interneurons over the course of development.

Cell sorting and microarrays. To gather sufficient cells for microarray screens, acute 400 μm coronal brain slices were prepared from G42 mice ($n = 3$ animals for each age) over a range of maturational time points: P7, P10, P13–P15, P25, and P40–P45. Brain slices were incubated in a protease solution (1 mg/ml Pronase E; Sigma-Aldrich) for ~1 h, after which time the somatosensory cortex was microdissected under a dissecting microscope. Microdissected tissue was then triturated in artificial CSF (ACSF) using a series of three Pasteur pipettes of decreasing tip diameter. The cell suspension was then poured into a small Petri dish, and, under visual control on a fluorescence dissecting microscope, GFP-expressing neurons were aspirated into a micropipette with a 30–50 μm tip diameter and transferred to a clean dish. After undergoing three such "washes," the sample was then lysed in 50 μl of extraction buffer (PicoPure RNA isolation kit; Arcturus), incubated at 42°C for 30 min, and then stored at −20°C. For a more detailed discussion of the sorting procedure, see Hempel et al. (2007). The mRNA from sorted cells was subsequently isolated, amplified, labeled, and hybridized to Affymetrix M430 2.0 arrays, as described in the Affymetrix GeneChip Eukaryotic Small Sample Target Labeling Assay Version 2. mRNA isolated from ~50–80 cells yielded sufficient quantities of labeled cRNA (10–80 μg). Arrays were scanned on an Affymetrix GeneChip scanner.

Analysis of microarray data. Scanned microarray data were processed with Affymetrix GeneChip Operating Software to convert raw image files (.DAT) to probe signal value files (.CEL). Probe signal values were then normalized and summarized using the Bioconductor affy package gcrma algorithm (http://www.bioconductor.org/packages/2.0/bioc/html/affy.html). We computed the maximum fold change for each gene by averaging the signal values across replicates for each time point and then computing the fold change between the maximum (max) and minimum (min) value, given by the formula $2^{(\max - \min)}$. Only genes showing a minimum of twofold change over development were included in additional analysis. To detect differentially expressed genes, we computed ANOVA p values for each gene using the R statistics package (http://www.r-project.org) and custom Python code. In cases in which a given gene corresponded to multiple probe sets on the array, we selected the probe set with the lowest p value. Principal component analysis (PCA) and k-means clustering were performed using Matlab (MathWorks). PCA was performed on the $m \times n$ data matrix ($m = 1973$; $n = 5$), in which each row corresponds to a developmentally regulated gene and each column corresponds to the signal value for each time point averaged across biological replicates and normalized to the range 0 (minimum) to 1 (maximum). The principal components are the eigenvectors derived from the $n \times n$ covariance matrix of developmental time points. p values for gene ontology (GO) overrepresentation analysis were calculated using the hypergeometric probability distribution to compute the probability of finding a given GO term in a list of arbitrary size, given the total number of genes on the Affymetrix GeneChip annotated with that term. Agglomerative hierarchical clustering analysis (supplemental Fig. 1*c*, available at www.jneurosci.org as supplemental material) was performed in R using the "agnes" function, with the Euclidean distance between gene expression profiles used as a metric. Microarray data for additional cell types used in supplemental Figure 1, *a* and *c* (available at www.jneurosci.org as supplemental material), and the middle panel of Figure 6*a* comes from Sugino et al. (2006). G30CG and G30S1 are mostly cholecystokinin-expressing irregular spiking interneurons from cingulate and somatosensory cortex, respectively, labeled in a transgenic mouse expressing GFP under a Gad2 promoter. GIN and GINH are somatostatin-expressing regular-spiking interneurons from cingulate cortex and hippocampus, labeled in a transgenic mouse expressing GFP under a GAD1 promoter. G42LG cells were extracted from the lateral geniculate nucleus in the thalamus. The YFPH mouse line is a transgenic line in which yellow fluorescent protein (YFP) is expressed under the control of the Thy1 promoter. YCG and YS1 are layer 5 pyramidal neurons from cingulate and somatosensory cortex, respectively. YH cells are YFPH cells extracted from the hippocampus, and YA are YFPH cells extracted from the amygdala. Finally, CT6 are layer six corticothalamic projection neurons labeled by injection of a retrograde tracer. Developmental G42 expression data as well as data for additional cell types are available at http://mouse.bio.brandeis.edu/.

Electrophysiology. Acute brain slices were prepared from G42 mice at ages corresponding to those used for microarray screens (P7, P10, P15, and P25) as described previously. Briefly, animals were deeply anesthetized with isoflurane and decapitated, and 300 μm coronal sections containing the primary somatosensory cortex (S1) were prepared on a vibratome in oxygenated ice-cold ACSF containing the following (in mM): 126 NaCl, 3 KCl, 2 $MgSO_4$, 1 NaH_2PO_4, 25 $NaHCO_3$, and 2 $CaCl_2$ (osmolarity adjusted to ~320 mOsm with dextrose, typically 10–15 mM). Slices were incubated at 37°C for 10–15 min and then at room temperature for at least another 30 min. For current-clamp recordings, slices were perfused continuously with 33–35°C ACSF supplemented with 50 μM D,L-2-amino-5-phosphonovaleric acid (APV) and 20 μM 6,7-dinitroquinoxaline-2,3-dione (DNQX) to block glutamatergic synaptic transmission and 50 μM picrotoxin to block ionotropic GABAergic transmission. For isolation of bupivacaine-sensitive currents, TTX, NiCl, nifedipine, ZD7288 (4-ethylphenylamino-1,2-dimethyl-6-methylaminopyrimidinium chloride), 4-AP, and tetraethylammonium were added to the recording ACSF (also maintained at 33–35°C) to block voltage-gated sodium, calcium, and potassium currents and I_H. The same mixture of drugs with the exception of NiCl and nifedipine was used during measurement and isolation of Ca^{2+} currents. Miniature synaptic events were recorded with TTX in the bath and either picrotoxin during miniature EPSC (mEPSC) recordings or DNQX and APV during mIPSC recordings. Whole-cell recordings were obtained from layer 5 G42 interneurons that were identified by GFP expression using standard epifluorescence and patched using Nomarski optics with pipettes that had a tip resistance of 5–12 MΩ when filled with internal solution containing the following: 100 mM K-gluconate, 20 mM KCl, 10 mM HEPES, 4 mM Mg-ATP, 0.3 mM Na-GTP, 10 mM Na-phosphocreatine, and 0.5% biocytin, adjusted to ~295mOsm with sucrose. For mIPSC recordings, we set E_{Cl} to 0 mV by using an internal solution containing the following: 133 mM KCl, 10 mM K-HEPES, 4 mM Mg-ATP, 0.3 mM Na-GTP, 2.5 mM Na-phosphocreatine, 0.5 mM EGTA, and 0.5% biocytin with sucrose added to adjust the osmolarity to ~295 mOsm. Input resistance was measured with 250 or 500 pA hyperpolarizing current injections at the beginning of every sweep in current clamp or by −5 mV voltage steps from the holding potential in voltage clamp. Series resistance was maintained below 20 MΩ or else the cell was discarded, and was compensated

75–85% in voltage-clamp recordings. Recordings in which the resting membrane potential or holding current, or the input resistance, drifted >20% during a recording were also discarded. The membrane potential was set to −70 mV with direct current injection at the beginning of each sweep during frequency–current (*F–I*) curves to equalize differences caused by the effect of different resting membrane potentials on inactivation of voltage-gated currents, although "natural" resting membrane potential was measured at the beginning of each current-clamp recording and approximately every 10 min thereafter. mEPSCs and mIPSCs were recorded at a holding potential of −70 mV. Signals were amplified by multiclamp 700A amplifiers (Molecular Devices) using the bridge balance in current-clamp recordings, digitized at 10 kHz, and stored on a hard drive using custom IGOR Pro (WaveMetrics) software. Voltage-clamp recordings were corrected *post hoc* for the measured junction potential of −10 mV.

Biocytin staining. Slices containing recorded G42 cells were fixed for <2 weeks in cold (4°C), buffered 4% paraformaldehyde. Biocytin was visualized by incubation with 1:500 Avidin D–Texas Red (Vector Laboratories) in 0.5% Triton X-100 for 1 h after permeabilizing the membrane with 1% Triton X-100 for 45 min and rinsing three times for 10 min each in PBS. Stained cells were examined on a dissecting microscope equipped with epifluorescence to verify the presence of both GFP and biocytin and to make gross morphological observations. In some cases, stained cells were further imaged at 63× on a confocal microscope.

Immunohistochemistry. G42 mice at P10 and P25 were deeply anesthetized with ketamine/xylazine/acepromazine and transcardially perfused with ice-cold 0.1 M PBS, followed by ice-cold 4% paraformaldehyde (PFA). Brains were postfixed for 24–100 h in 4% PFA and then embedded in agar and sectioned coronally at 50 μm on a vibratome. Sections containing S1 were stored at 4°C until staining. For TASK1 immunostaining, sections were washed with PBS, blocked in 10% horse or goat serum in 0.1 M PBS containing 1% Triton X-100 for 1 h, and incubated overnight at 4°C with 1:500 mouse anti-GFP (Millipore Bioscience Research Reagents) and 1:250 rabbit anti-TASK1 (Millipore Bioscience Research Reagents) in 0.1 M PBS supplemented with 0.1% Triton X-100 and 1% horse or goat serum. GFP and TASK1 antibodies were detected by incubation with 1:500 goat anti-mouse Alexa-488 and 1:500 goat anti-rabbit Alexa-568 in 0.1 M PBS with 0.1% Triton X-100 and 1% horse or goat serum for 2 h after the sections were washed three times in 0.1 M PBS. We stained P10 and P25 sections in parallel to avoid batch effects. TASK1 antibody specificity was verified by successfully preventing staining with preincubation of the antibody with the epitope it was raised against (CEDEK RDAEH RALLT RNGQ). Stained sections were imaged using a 40× objective on a confocal microscope, and the laser power, photomultiplier gain, pinhole, and detection filter settings were identical for P10 and P25 imaging sessions. TASK immunosignal was quantified in NIH ImageJ by averaging the TASK signal subsumed by each GFP-positive somata in two animals and two to three fields of view (FOVs) per age.

Results

We characterized the transcriptional and electrophysiological maturation of genetically labeled FS interneurons in mouse S1 cortex using whole-genome microarrays and whole-cell recordings. mRNA was harvested from manually sorted GFP-expressing neurons dissociated from acutely prepared brain slices at a range of developmental time points (P7, P10, P15, P25, and P40) and subsequently reverse transcribed, amplified, labeled, and hybridized to Affymetrix 430 2.0 whole-genome microarrays (three microarrays from three different animals per condition). To detect genes that are differentially expressed over the course of maturation, we performed an ANOVA across all samples for each of the ~45,000 probe sets represented on the chip. To refine our estimate of the number of differentially expressed genes, we also performed ANOVAs on shuffled datasets in which each sample was assigned to one of five triplicate groups at random (supplemental Fig. S2*a*, available at www.jneurosci.org as supplemental material). The resulting distributions of *p* values for each shuffled dataset were averaged and used to compute the false discovery rate as a function of ANOVA *p* value, which we defined as the ratio of the number of genes corresponding to a given *p* value in the shuffled versus the original dataset (supplemental Fig. S2*b*, available at www.jneurosci.org as supplemental material). By subtracting the two distributions, we obtained the "corrected" distribution of *p* values (Fig. 1*A*). We restricted our consideration of differentially expressed genes to those with $p < 10^{-3}$, which corresponded to a false discovery rate of 1%. The set of differentially expressed genes was further limited to those exhibiting a minimum twofold change in expression over development (Fig. 1*B*). A total of 1973 genes met the above criteria.

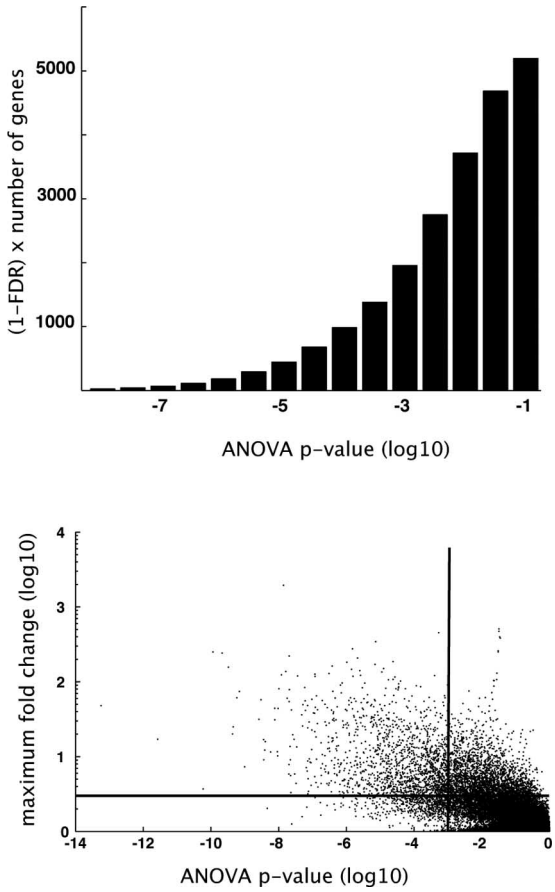

Figure 1. Number of developmentally regulated genes and dynamic range of regulation. ***A***, False discovery rate (FDR)-corrected frequency distribution of ANOVA *p* values. ANOVA *p* values were calculated for each gene across all measured time points (P7, P10, P15, P25, and P40, 3 microarrays per condition). The false discovery rate was estimated by subtracting the distribution of *p* values resulting from ANOVAs performed on randomly shuffled datasets. ***B***, ANOVA *p* values plotted against maximum fold change for each gene. Horizontal and vertical lines demarcate arbitrary cutoff values for fold change (2-fold) and ANOVA *p* value (10^{-3}), respectively.

To uncover patterns of developmental regulation, PCA and *k*-means clustering analyses were applied to the expression profiles of differentially expressed genes. To focus directly on the time course of regulation rather than the overall expression level of a gene, expression profiles of each gene were first normalized to the range 0 (minimum) to 1 (maximum). We found that the first and second principal components accounted for ~77 and 12% of the total variance, respectively. The first principle component can be interpreted as the slope of the change in expression level over time (Fig. 2*A*). Two clusters, corresponding to increasing and decreasing sets of genes, having positive and negative slope, re-

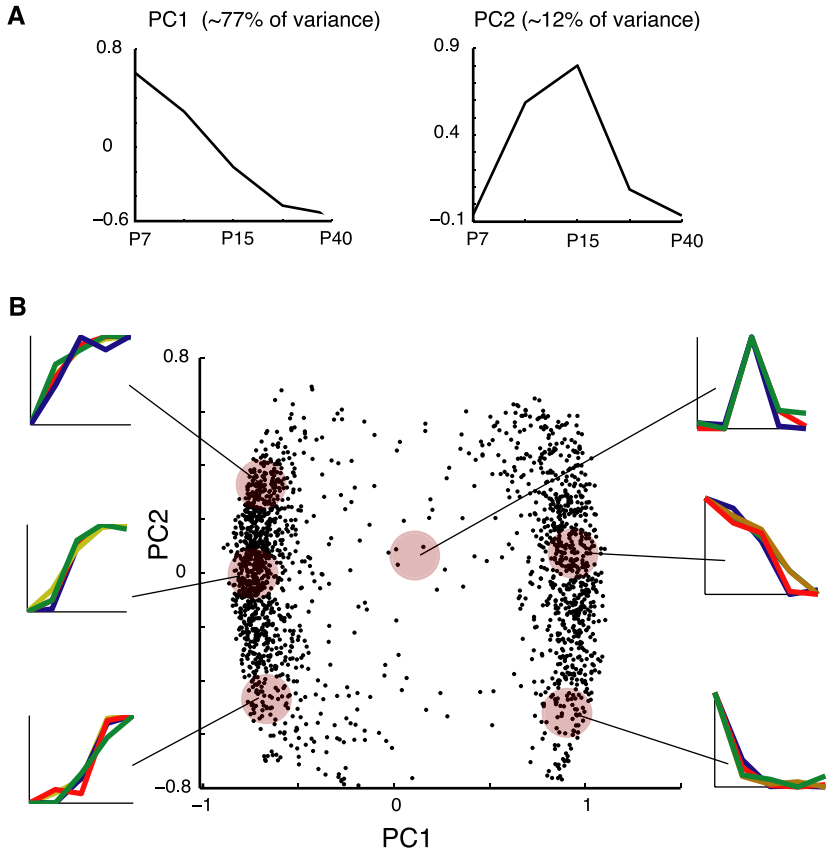

Figure 2. Developmentally regulated genes exhibit mostly monotonically increasing or decreasing trajectories. PCA was performed on all genes with an associated ANOVA p value of $<10^{-3}$ and a minimum twofold change in expression over development. Before performing PCA, expression profiles were normalized. ***A***, Plot of the first and second principle components, accounting for ~77 and ~12% of the total variance, respectively. ***B***, Plot of the first versus second principal component. Displayed trajectories are exemplars of the scaled expression trajectories of genes occupying a given region of PCA space, denoted by shaded discs.

spectively, are plainly discernible in the plot of the first versus the second principal component (Fig. 2*B*). This was consistent with *k*-means clustering that revealed that increasing the number of clusters beyond two resulted in diminishing silhouette values (data not shown). The second principal component contributed to the concavity or convexity of the expression trajectory (Fig. 2*A*). Increasing genes with positive second principal component coefficients are upregulated early in the course of maturation, whereas increasing genes with negative second principal component coefficients are upregulated much later in development (Fig. 2*B*, left). Alternatively, decreasing genes with positive second principal component coefficients were downregulated much later than decreasing genes with negative coefficients (Fig. 2*B*, right). The continuous distribution of points along the second principal component axis indicates that the interval of greatest change between time points varied continuously across individual gene expression profiles. Very few genes had large second component coefficients but small first component coefficients (Fig. 2*B*, middle), indicating that expression trajectories that peaked or troughed at intermediate time points and then sharply declined or increased were less frequently observed. Thus, developmental regulatory patterns of gene expression were primarily monotonically increasing or decreasing. GO overrepresentation analysis revealed enrichment of specific functional categories among upregulated and downregulated transcripts (Table 1). Seven of the 10 most significantly enriched GO terms ($p < 10^{-5}$) were associated with ion channel activity. Overall, 27 ion channels were upregulated and 13 ion channels were downregulated over the course of maturation (Fig. 3). In particular, voltage-gated potassium channels were enriched among upregulated genes, whereas voltage-gated sodium channels and voltage-gated calcium channels were overrepresented in the set of downregulated genes.

These developmental changes in ion channel expression likely manifest as corresponding changes in G42 intrinsic membrane properties. We therefore characterized G42 electrophysiological maturation by performing whole-cell current-clamp recordings in the presence of synaptic blockers from identified G42 cells in acute cortical slices containing primary motor cortex and S1 at P7, P10, P15, and P25. The mature FS phenotype is characterized by high firing rates (>200 Hz), narrow spikes relative to other neocortical cell types, and little or no spike-frequency adaptation (McCormick et al., 1985) (Fig. 4, rightmost trace). Consistent with previous studies of FS interneuron development in layer 4 (Itami et al., 2007) and in dentate gyrus (Doischer et al., 2008), we found that these mature features emerged slowly and monotonically over development (Fig. 4) and that immature G42 neurons are electrophysiologically distinct from the mature state. The characteristic lack of adaptation during repetitive firing, for instance, emerged between P10 and P15, and G42 cells at P7 exhibited pronounced and robust spike-frequency adaptation (measured as the ratio of first to last interspike intervals: 0.72 ± 0.12 at P7, 1.05 ± 0.30 at P15; $p < 0.05$). Consistent with this loss of adaptation, our microarray results revealed a 15-fold downregulation of the small conductance Ca^{2+}-activated K^+ channel *Kcnn2*, which contributes to the medium component of the afterhyperpolarization after an action potential in multiple cell types (Bond et al., 2004; Kong et al., 2008; Liu and Herbison, 2008). Moreover, the kinetics of this current are consistent with the kinetics of adaptation we observed in immature G42 neurons, suggesting that expression of *Kcnn2* may underlie spike-frequency adaptation in these cells. The emergence of the non-adapting firing phenotype was accompanied by an increase in maximum firing rate, which increased nearly threefold from P7 to P25 ($p < 10^{-4}$) and surprisingly increased by 20% between P15 and P25 ($p < 0.01$), indicating that even the most prominent features of mature FS cells undergo substantial developmental regulation as late as the second postnatal week. Unsurprisingly, we also found that spike width, measured between spike threshold and the end of the spike, was inversely correlated with maximum firing rate and decreased from 3.6 ms at P7 to 2.3 ms at P25 ($p < 10^{-4}$). It has been demonstrated that Kv3 potassium channels encoded by *Kcnc1* and *Kcnc2* enable sustained fast spiking by providing rapid repolarization of the membrane potential after an action potential (Du et al., 1996; Erisir et al., 1999; Lau et al., 2000; Rudy and McBain, 2001). Concordantly, we found that these transcripts were upregulated

Table 1. GO overrepresentation analysis reveals enrichment of specific categories of molecular function among developmentally upregulated (top) and downregulated (bottom) genes

GO term (molecular function)	*p* value	Found/total
Upregulated genes		
Transporter activity	0.004	101/1454
Channel or pore class transporter activity	0.003	34/386
Ion transporter activity	8×10^{-6}	62/655
Ion channel activity	2×10^{-4}	34/330
Voltage-gated ion channel activity	2×10^{-6}	25/163
Voltage-gated potassium channel activity	6×10^{-5}	16/98
Cation channel activity	3×10^{-5}	29/237
Potassium channel activity	2×10^{-5}	20/130
Metal ion transporter activity	0.003	11/77
Cation transporter activity	4×10^{-6}	53/518
Potassium ion binding	5×10^{-4}	14/95
Magnesium ion binding	5×10^{-5}	32/281
Catalytic activity	5×10^{-5}	311/4879
Oxidoreductase activity, acting on NADH or NADPH	0.007	9/64
Kinase activity	0.007	65/890
Inositol or phosphatidylinositol phosphatase activity	0.008	6/33
Phosphoinositide 5-phosphatase activity	0.001	3/5
Acetylglucosaminyltransferase activity	0.004	5/21
Downregulated genes		
Protein binding	1×10^{-4}	207/3733
RNA binding	6×10^{-5}	44/533
Calmodulin binding	0.002	12/105
Cytoskeletal protein binding	5×10^{-5}	31/325
Structural constituent of ribosome	2×10^{-4}	23/228
Oxidoreductase activity, acting on paired donors	4×10^{-4}	4/9
Calcium channel regulator activity	0.002	4/13
Voltage-gated calcium channel activity	0.009	4/19
Voltage-gated sodium channel activity	0.001	4/12

Hierarchical relationship of GO terms is denoted by indentation. *p* values were calculated using the hypergeometric probability distribution, which computes the probability of finding a given GO term in the list of differentially expressed genes (found), given the total number of genes on the Affymetrix GeneChip annotated with that term (total). All terms with $p < 0.01$ are shown.

over the same developmental interval (*Kcnc1*, ~14-fold increase; *Kcnc2*, ~2-fold increase).

In addition to the developmental loss of spike-frequency adaptation, narrowing of action potentials, and concomitant emergence of high-frequency firing, we also found a massive and highly significant decrease in the input resistance (R_{In}) of G42 cells over development. Although the slope and saturation point of the *F–I* curve increased as G42 cells matured, the amount of current required to elicit action potentials also increased nearly eightfold from P7 to P25 ($p < 10^{-6}$) and 2.6-fold from P15 to P25 ($p < 10^{-4}$). This dramatic increase in rheobase over development is consistent with previous reports in interneurons (Itami et al., 2007; Doischer et al., 2008) and pyramidal cells (Maravall et al., 2004; Zhang, 2004) and, in this case, is likely attributable in part to a decrease in resting R_{In} between P7 and P10 (537.4 ± 27.3 MΩ at P7, 155.0 ± 27.3 MΩ at P10; $p < 10^{-4}$) and between P15 and P25 (126.7 ± 35.3 MΩ at P15, 70.6 ± 14.2 MΩ at P25; $p < 0.01$), as well as to a positive shift in the action potential voltage threshold between P7 and P15 ($p < 0.05$). The membrane time constant (τ_M), a crucial determinant of the integrative properties of a neuron, also decreased precipitously from 35.4 ± 7.7 ms at P7 to 2.8 ± 0.9 ms at P25 ($p < 10^{-7}$), as would be expected given the close relationship between R_{In} and τ_M and the lack of a significant difference in whole-cell capacitance across ages (data not shown).

The parallel increase in rheobase and decrease in resting R_{In} suggest that both may be mediated in part by developmental upregulation of potassium leak channels, because we measured R_{In} by inducing small (<5 mV) hyperpolarizing voltage deflections from the resting membrane potential. In this regime, the membrane potential and input resistance are primarily governed by background leak currents and voltage-gated currents such as I_H and I_{Kir} that are active at relatively hyperpolarized voltages. A search of potassium leak channel transcripts that our microarray screen indicated were upregulated over development revealed that *Kcnk3*, which codes for the two-pore potassium leak channel TASK1, and *Kcnk1*, which codes for the two-pore leak channel TWIK1 (Lesage and Lazdunski, 2000), are both highly enriched in p25 G42 interneurons compared with those isolated from younger animals (~13-fold and ~5-fold, respectively). Two-pore potassium leak conductances are blocked by the local anesthetic bupivacaine (Kindler et al., 1999; Torborg et al., 2006). We therefore directly measured TWIK1 and TASK1 function over development by pharmacologically isolating TWIK1 and TASK1-mediated leak currents in P10, P15, and P25 G42 interneurons with 40 μM bupivacaine in the presence of voltage-gated potassium, sodium, and calcium channel blockers. Bupivacaine blocked a voltage-insensitive current that reversed close to the calculated potassium equilibrium potential in cells from all three ages, and the magnitude of this current increased 5.7-fold between P7 and P25 over development ($p < 0.01$) (Fig. 5). Moreover, the contribution of the bupivacaine-sensitive conductance to the whole-cell conductance that remained after blockade of voltage-gated K^+, Na^+, and Ca^{2+} channels also increased significantly between each age tested (Fig. 5*B*), indicating that two-pore K^+ leak channels become increasingly important determinants of G42 R_{In} over postnatal development.

If the increase in bupivacaine-sensitive current is indeed at-

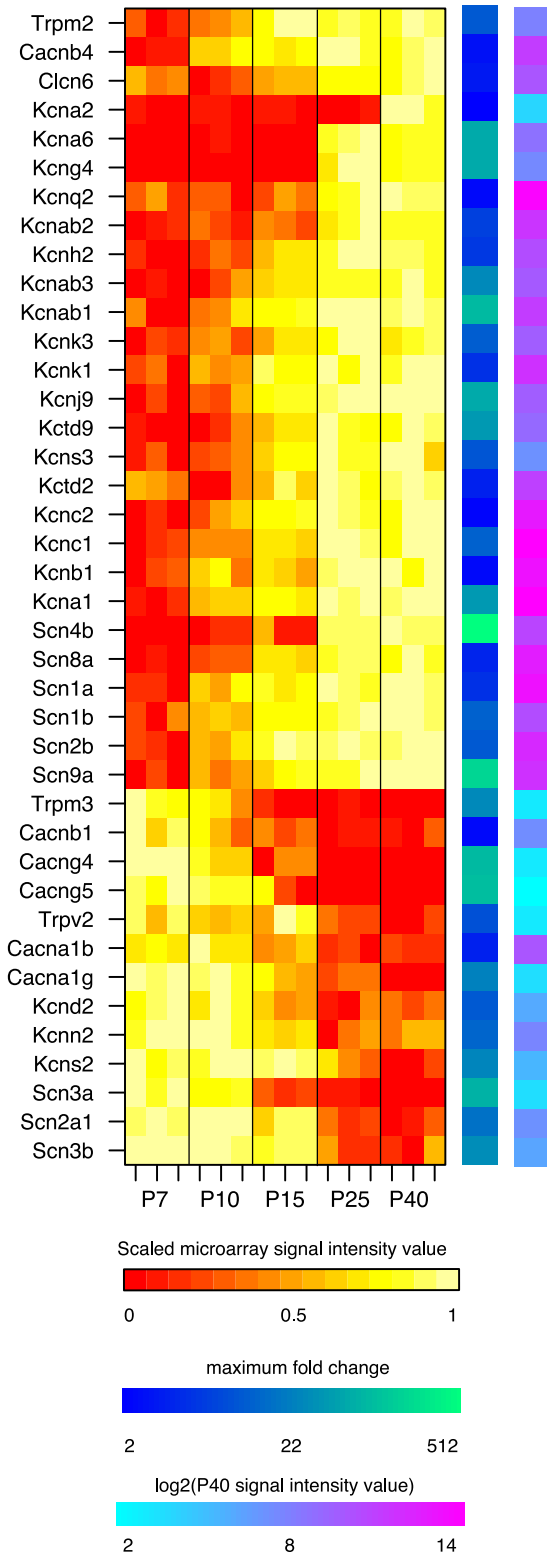

Figure 3. Developmentally regulated ion channels. Heat maps denote (from left to right) the scaled microarray signal intensity, the maximum fold change, and log2 of the P40 microarray signal intensity value for each gene. Genes at the top are upregulated, and genes at the bottom are downregulated.

tributable to increased TASK1 protein expression, as one might predict given the enrichment of *Kcnk3* transcript in older animals, TASK1 immunocytochemistry should differ between ages. We immunolabeled TASK1 in sections taken from P10 and P25 G42 animals and quantified the intensity of TASK1 label in GFP-labeled G42 interneurons (Fig. 5). TASK1 immunoreactivity in regions coextensive with GFP-labeled somata was almost twofold more frequent ($\text{overlap}_{P10} = 0.47$; $\text{overlap}_{P25} = 0.91$; $p < 10^{-4}$) and stronger at P25 than at P10 ($\text{intensity}_{P10} = 28.6 \pm 4.1$; $\text{intensity}_{P25} = 50.1 \pm 5.7$; $p < 10^{-6}$) (Fig. 5*B*).

The observed increase in the magnitude of injected current required to elicit action potentials may also reflect the upregulation of voltage-gated outward currents active between resting membrane potential and voltage threshold in mature versus developing FS cells. Our microarray screen detected increased expression of multiple Kv1-type potassium channel subunit transcripts known to reduce neuronal excitability. *Kcna1* and *Kcna6*, as well as the *Kcnab1*, *Kcnab2*, and *Kcnab3* modulatory subunits, all show striking upregulation over the course of maturation (~44-fold, ~61-fold, ~86-fold, ~7-fold, and ~33-fold, respectively). Together, these results show that immature G42 FS interneurons are initially highly excitable, integrate inputs over long (~35 ms) time windows, and respond to sustained input with relatively low-frequency adapting spike trains and that over the next 2 weeks of development FS cells become progressively and dramatically harder to excite, sensitive only to coincident input, and capable of very high-frequency repetitive firing without adaptation once driven past threshold.

Although Kv3 potassium channels enable the sustained high-frequency firing of FS cells, and Kv1 potassium channels, together with an assortment of potassium leak channels, likely control their excitability, sodium channels are indispensable for membrane depolarization necessary for the initiation of action potentials. With this in mind, it is perhaps unexpected that sodium channel transcripts are overrepresented among downregulated genes. *Scn3a*, *Scn2a1*, and *Scn3b* all exhibit decreasing developmental expression trajectories (~74-fold, ~20-fold, and ~35-fold, respectively). Although sodium channel genes are not significantly overrepresented in the set of upregulated genes, the expression levels of six transcripts encoding voltage-gated sodium channel subunits increase significantly over the course of maturation: *Scn4b*, *Scn8a*, *Scn1a*, *Scn1b*, *Scn2b*, and *Scn9a* (~344-fold, ~4-fold, ~5-fold, ~14-fold, ~12-fold, and ~146-fold, respectively). This bidirectional regulation suggests that the expression of different sets of sodium channels may be required for immature versus mature functions.

Just as the regulation of potassium and sodium channels plays a crucial role in determining the excitability of G42 FS cells, regulation of calcium channels and of calcium homeostasis in general also appear to be salient components of G42 FS cell maturation. Seven of the 13 downregulated ion channel subunits form or associate with channels that flux calcium: *Cacng5*, *Cacng4*, *Trpm3*, *Cacna1g*, *Trpv2*, *Cacna1b*, and *Cacnb1* (~89-fold, ~84-fold, ~33-fold, ~28-fold, ~10-fold, ~4-fold, and ~2-fold, respectively). In particular, downregulation of the T-type calcium channel $Ca_v3.1d$, encoded by the *Cacna1g* gene, by virtue of its low-voltage threshold for activation, likely contributes to the maturational attenuation of excitability we observed in G42 FS cells (Iftinca and Zamponi, 2009). Indeed, we recorded TTX-insensitive humps and action potentials in P7 G42 FS cells (nine of nine) that were abolished by bath application of the T-type Ca^{2+} channel blocker nickel (100 μm; three of three cells), and, in two of these cells, we isolated a nickel-sensitive T-type current in voltage clamp (supplemental Fig. S3, available at www.jneurosci.org as supplemental material). In contrast, we never observed spiking behavior in the presence of TTX at P25.

Downregulation of channels that are permeable to calcium

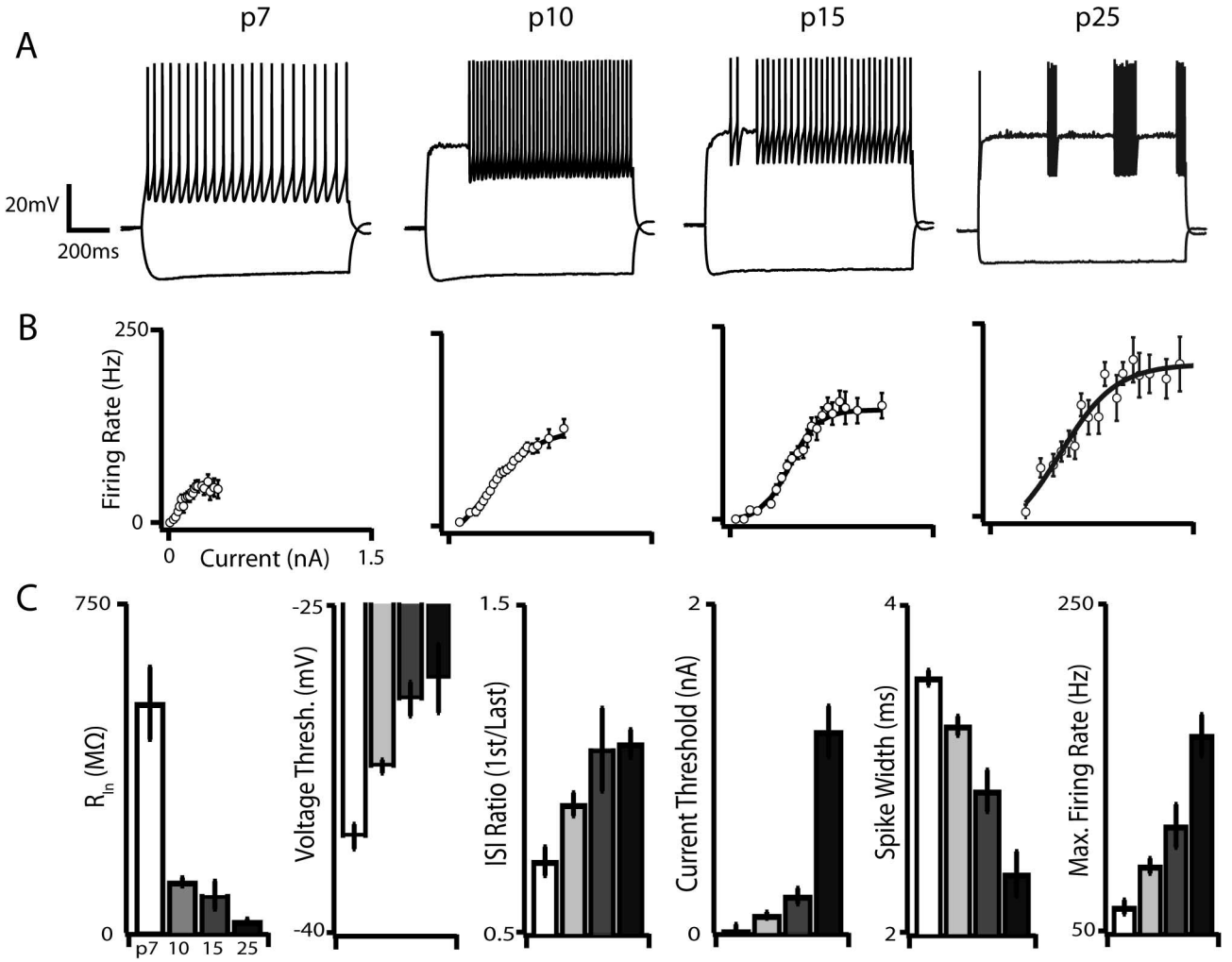

Figure 4. Maturation of intrinsic membrane properties and the distinctive firing type of G42 FS interneurons. ***A***, Representative voltage traces from each developmental point. Current injections were 90 pA (P7), 160 pA (P10), 300 pA (P15), and 580 pA (P25). Action potential trains are initially adapting but lose this property by P10, and the membrane becomes progressively less excitable. Also note the onset of "stuttering" spike trains evoked by threshold current injections at P10. ***B***, Population *F–I* curves at each developmental point. Both current threshold and maximum firing rate increase dramatically over development. ***C***, Summary data for input resistance (R_{In}), voltage threshold, adaptation index (interspike interval ratio), current threshold, spike width, and maximum firing rate at each developmental point. All of these parameters progress monotonically over development. Error bars here and in other figures indicate SEM unless otherwise noted.

may help G42 FS cells control their intracellular calcium concentration in the face of dramatic increases in firing rates over development that presumably increase calcium entry through voltage-gated channels. Regulatory patterns of other genes involved in calcium homeostasis lend additional support to this hypothesis. For instance, the calcium-buffering molecule parvalbumin is upregulated nearly 30-fold between P10 and P40. Additionally, the Ca^{2+}-ATPase, encoded by the *Atp2b3* gene, which extrudes calcium ions from the cell, is upregulated fourfold between P7 and P25. In addition to influencing cell excitability, calcium plays a critical role as a signaling molecule whose downstream effects mediate a host of cellular processes, including cell differentiation and synaptic plasticity, often by inducing transcriptional modifications (Moody and Bosma, 2005; Flavell and Greenberg, 2008). Thus, mechanisms that promote calcium entry early in development may be necessary for cell differentiation and may be distinct from calcium sources required for the subsequent maintenance of mature cell identity.

Changes in the abundance of transcripts for ion channels and other genes likely reflect changing patterns of transcriptional regulation. It is known that PV-expressing FS cells derive from *Nkx2.1*-expressing progenitors in the medial ganglionic eminence and that subsequent expression of the transcription factors *Dlx1*, *Lhx6*, and *Arx* is necessary for proper PV-subtype migration and differentiation (Alifragis et al., 2004; Liodis et al., 2007; Colasante et al., 2008; Friocourt et al., 2008; Zhao et al., 2008). However, the downstream targets of these transcription factors, and the identity of other transcription factors arising at later stages of development, have yet to be fully elucidated (Fulp et al., 2008). Our data provide candidate transcription factors that may be essential to the maturation and maintenance of cell identity (Fig. 6*A*). In particular, we identified several transcription factors that were upregulated in concert with the emergence of mature phenotype and that appear to show stable expression in the adult, such as *Lmo2*, *Etv5*, *Pbx3*, A630082k20Rik, *Ankrd25*, *Zf*, *Nfkbie*, and *Cbx7*. Expression of some of these is enriched in adult G42 cells with respect to other cell types (Sugino et al., 2006). Other previously characterized transcription factors known to figure prominently in the early development of interneuron subtypes were markedly downregulated, such as *Sox11*, *Sox4*, *Myc*, and *Ascl1*, suggesting that they play no role in the maintenance of FS interneuron identity. In accordance with the developmental

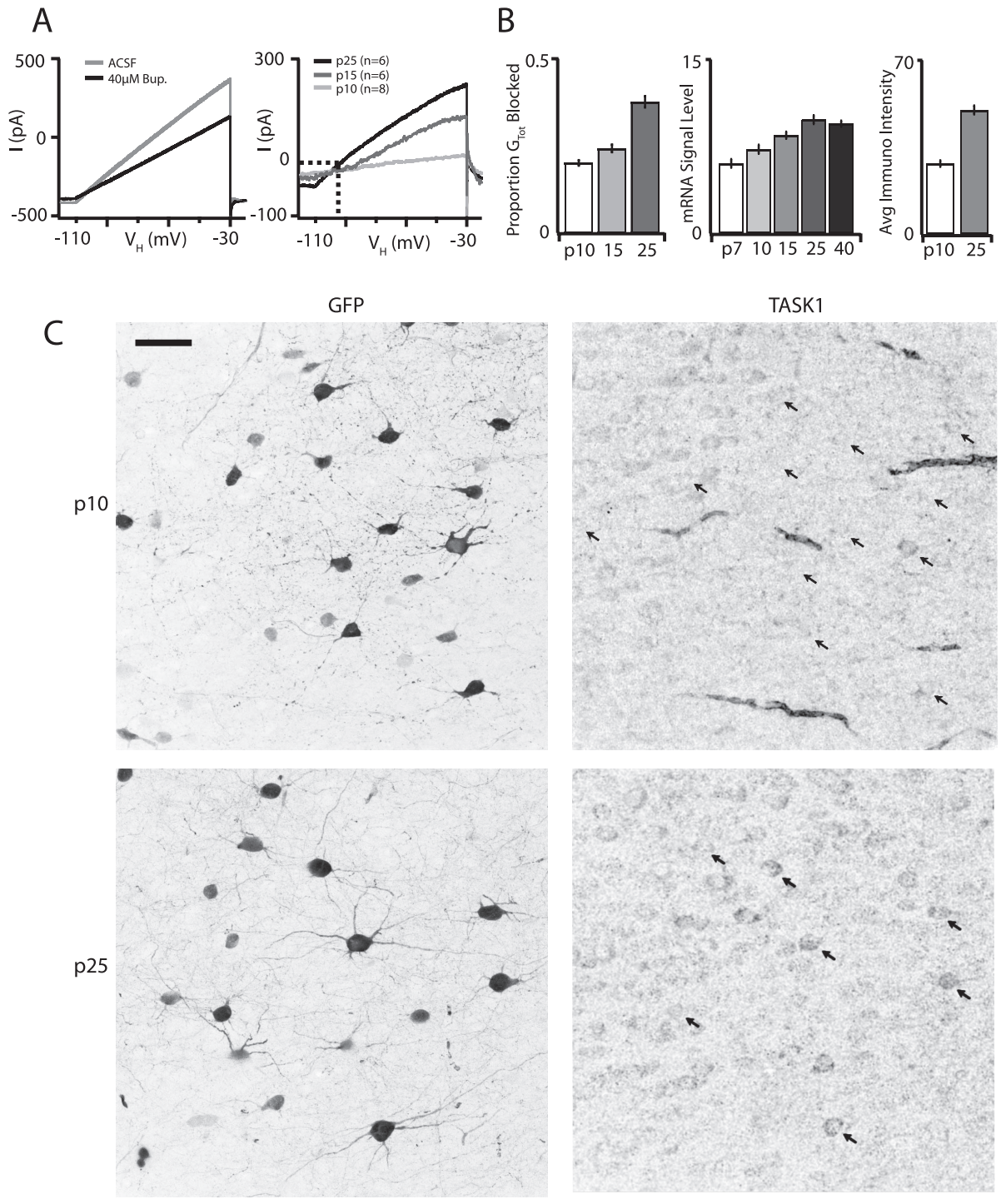

Figure 5. The two-pore potassium leak channels TWIK1 and TASK1 are upregulated in G42 FS interneurons over postnatal development and exert increasing influence on membrane excitability. ***A***, Average whole-cell currents evoked by a voltage ramp from −110 to −30 mV at P25 before and after bath application of 40 μM bupivacaine (left). Average bupivacaine-sensitive currents at P7, P10, and P25. Dashed lines indicate zero current and the potassium equilibrium potential (E_K, right). ***B***, Bupivacaine-sensitive conductances account for a greater proportion of the whole-cell resting conductance as G42 FS interneurons mature (left). Right panels represent the increasing developmental trajectory of *kcnk3* transcript levels measured by microarray and TASK1 protein detected by immunostaining. ***C***, Immunostaining for TASK1 at P10 (top row) and P25 (bottom row). G42 FS interneurons are labeled with GFP, and the amount and intensity of TASK1 signal coextensive with GFP signal both increase between P10 and P25. Arrows in the TASK panels indicate the location of G42 somata in the same FOV. Scale bar, 40 μm.

function of these transcription factors, GO overrepresentation analysis showed that genes associated with nervous system development, cell proliferation, neuron differentiation, and axon guidance were enriched in the set of downregulated genes (supplemental Table 1, available at www.jneurosci.org as supplemental material). Interestingly, *Dlx1*, *Lhx6*, and *Arx* show stable expression over the course of maturation, implicating them in persistent regulatory roles. Developing and mature G42 cells also stably express the transcription factor *Sox2*, which is expressed in several mature interneuron populations (Sugino et al., 2006) and may play a role in the development of GABAergic cells as well (Cavallaro et al., 2008).

In addition to refining their intrinsic physiological properties, G42 FS cells also refine their synaptic properties over the course of maturation. We detected transcriptional regulation of an assortment of cell adhesion molecules presumed to play a role in synaptic connectivity, as well as migration and differentiation, such as *Ncam2*, *Clstn3*, *Farp2*, *Bcan*, *Hapln4*, *Hapln1*, *Vcan*, *Ncan*, Chl1, *Nxn1*, *Cxadr*, and *Fat4* (Fig. 6*B*,*C*). Among these cell adhesion genes, several are involved in the formation of perineuronal nets (PNs) (Fig. 6*B*). The chondroitin sulfate proteoglycans aggrecan (*Agc1*), versican (*Vcan*), neurocan (*Ncan*), and brevican (*Bcan*), together with the hyaluronan and proteoglycan binding link proteins (*HAPLN*s) have been identified as structural components of PNs in the rodent brain (Deepa et al., 2006). *Agc1* is stably expressed by G42 cells from P7 onward (supplemental Fig. S1*b*, available at www.jneurosci.org as supplemental material), but *Vcan*, *Ncan*, and *Bcan*, as well as *HAPLN4* and *HAPLN1* are all developmentally regulated (~80-fold downregulated, ~13-fold downregulated, ~16-fold upregulated, ~127-fold upregulated, and ~116-fold upregulated, respectively). Additionally, *ADAMTS5*, *ADAMTSl5*, *ADAMTS8*, and *ADAMTS20*, all members of the ADAMTS family of glutamyl-endopeptidases that break down proteoglycans and thereby degrade PNs, are also developmentally regulated (~18-fold downregulated, ~58-fold upregulated, ~94-fold upregulated, and ~6-fold downregulated). Given that the formation of PNs may inhibit neural plasticity (Galtrey and Fawcett, 2007; McRae et al., 2007; Hamel et al., 2008), bidirectional regulation of both proteoglycans and proteoglycan-degrading genes suggests that different plasticity rules may operate at different times during development. Additionally, filtering the set of differentially expressed genes for the GO term "synaptic activity related" selected 17 genes, 10 upregulated and 7 downregulated (Fig. 6*D*). Many of the upregulated genes are involved in the presynaptic release of neurotransmitter, such as *Syt2*, *Syn2*, *Rab3a*, *Syngr1*, and *Sv2a*.

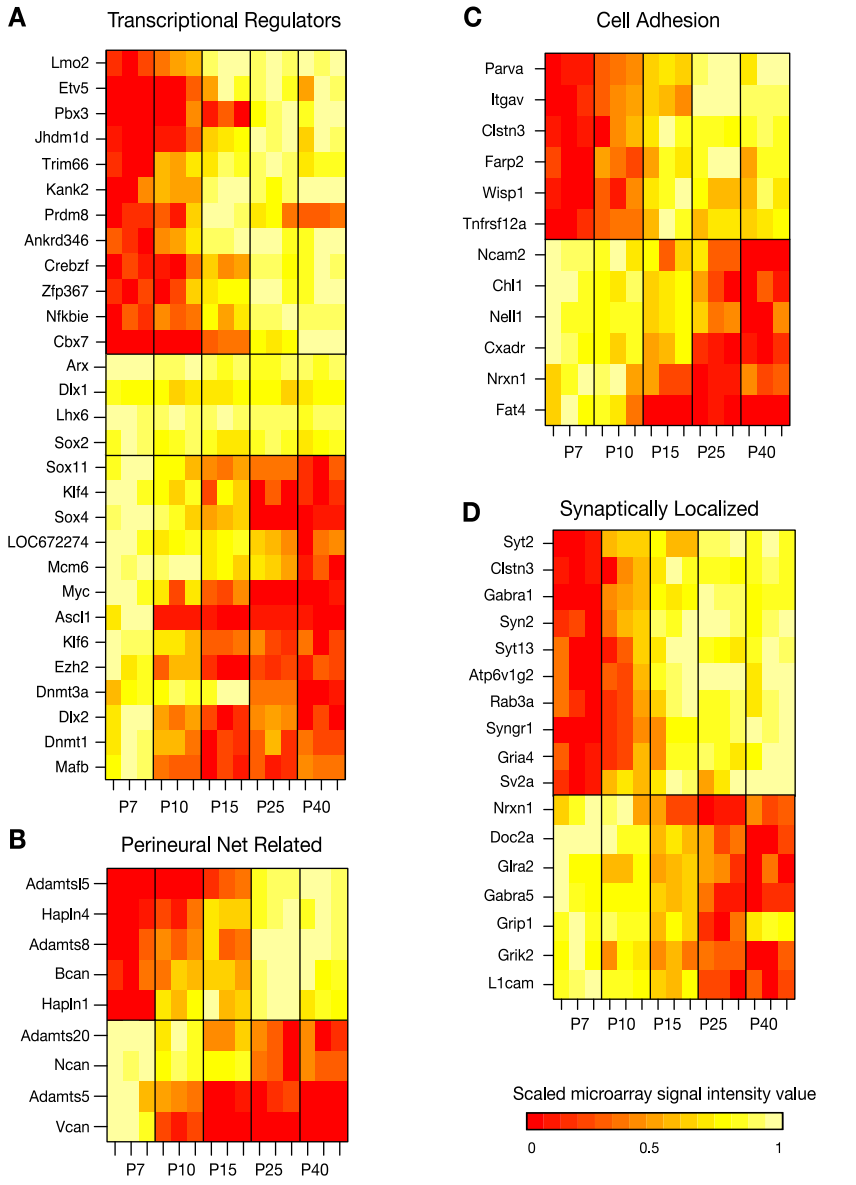

Figure 6. Developmentally regulated genes related to the following: ***A***, transcriptional regulation; ***B***, perineural nets; ***C***, cell adhesion; and ***D***, synaptic function. Heat maps denote the scaled microarray signal intensity. Given that scaling to the maximum and minimum value of a signal that is not significantly changing will amplify small perturbations from the mean and thereby give the appearance of dynamic regulation, signal values for stably expressed interneuron-specific transcription factors in the middle panel of ***A*** were scaled across microarray signal values from multiple cortical cell types (see Materials and Methods).

We also measured developmental changes in excitatory and inhibitory synaptic input to G42 FS cells by recording mEPSCs and mIPSCs in voltage clamp. Both the amplitude and frequency of mEPSCs and mIPSCs increased dramatically over development, although mEPSC amplitude and frequency peaked at P15 and then decreased slightly, whereas mIPSC amplitude and frequency increased monotonically and peaked at P25 and P15, respectively (Figs. 7, 8). The largest increases in mPSC frequency occurred between P7 and P10 for both mIPSCs (5.6-fold) and mEPSCs (5.38-fold), and, at all developmental time points except P25, the frequency of mEPSCs was greater than that of mIPSCs (Fig. 7*C*). Interestingly, although the mEPSC decay time constant (τ_{Decay}) decreased only marginally over development (1.2-fold between P10 and P15; $p < 0.01$), mIPSC τ_{Decay} decreased almost 10-fold between P7 ($\tau_{Decay} = 21.6$ ms) and P25 ($\tau_{Decay} = 2.7$ ms; $p < 10^{-6}$). This developmental decrease in mIPSCs τ_{Decay} has been reported previously in cortical pyramidal cells (Dunning et al., 1999), in which it is attributable to upregulation of the α1 and downregulation of the α5 $GABA_A$ receptor subunits. In these neurons, mIPSC τ_{Decay} is inversely related to the ratio of α1 to α5 subunits (Dunning et al., 1999). Our data are consistent with the idea that this switch also occurs in G42 FS interneurons. The *gabra1*/*gabra5* ratio measured by our microarray screen increased 61-fold between P7 and P25 and was inversely correlated with the trajectory of mIPSC τ_{Decay} (Fig. 8*C*), suggesting that developmental sharpening of inhibitory transmission attributable to this $GABA_A$ receptor subunit switch may be a general property of multiple neocortical cell types.

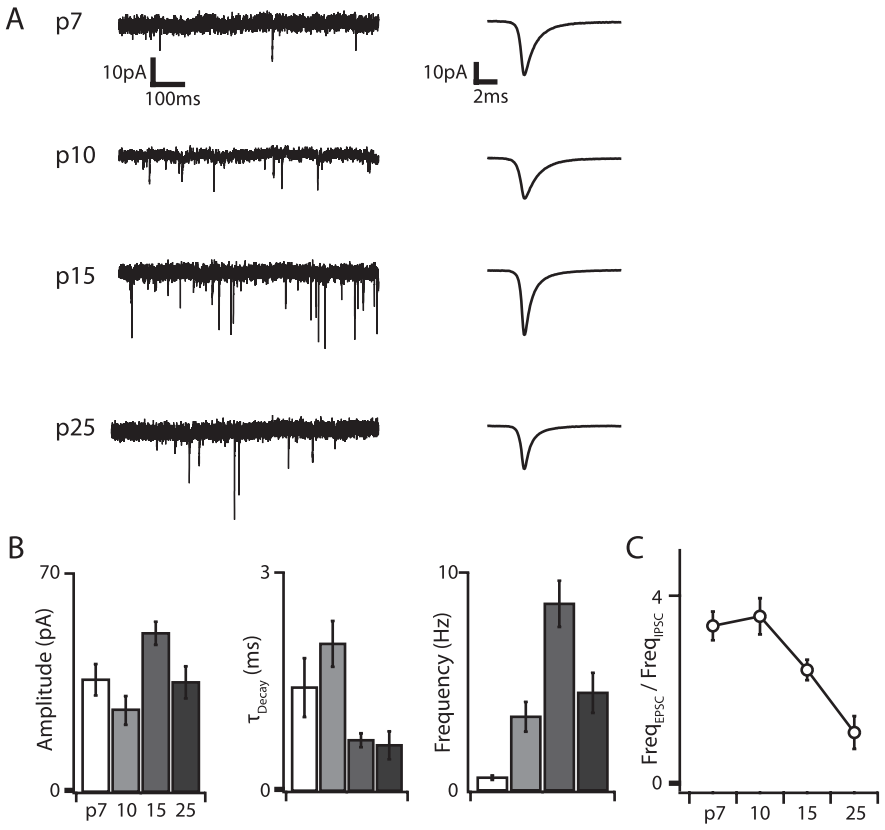

Figure 7. Excitatory synaptic transmission undergoes extensive and non-monotonic maturation between P7 and P25. ***A***, Representative current traces obtained at V_{Hold} of −70 mV in the presence of $GABA_A$ receptor blockers and TTX at each age and corresponding average mEPSC waveforms (rightmost traces). Note the marked increase in mEPSC frequency over development. ***B***, Summary data for mEPSC amplitude, decay time constant, and frequency. Both amplitude and frequency reach maxima at P15 and decline slightly by P25. ***C***, The ratio of mEPSC to mIPSC frequency is large (~4) early in development but decreases to ~1 by P25, suggesting that excitatory inputs outweigh inhibitory ones for much of postnatal development in G42 FS interneurons.

Discussion

We measured changes in whole-transcriptome expression and in the
intrinsic and synaptic physiology of genetically labeled cortical fast-spiking parvalbumin-expressing GABAergic interneurons over the first 6 postnatal weeks. Previous studies have assayed whole-transcriptome expression in rodent neocortex over similar periods of maturation (Semeralul et al., 2006; Stead et al., 2006; Lyckman et al., 2008), but ours is the first to restrict such analysis to a homogeneous subclass of interneurons. In so doing, we were able to reveal cell-type-specific transcriptional changes that are not readily extricable from the overall transcriptional profiles of complex tissues such as the cerebral cortex. We found that 1972 genes were differentially expressed over the span of P7–P40 and that 1124 genes showed an increase in expression, whereas 848 genes showed a decrease. Non-monotonic expression trajectories were rarely observed. This is in contrast to earlier periods of development in which critical sets of genes are often transiently upregulated and then downregulated as their transitory developmental functions run their course (Lieuw et al., 1997; Shirasaki and Pfaff, 2002; Guillemot et al., 2006; Wonders and Anderson, 2006). Our observations likely reflect the shutdown of developmental programs initiated before P7, concomitant with the onset and progression of the transcriptional maturation of G42 cells.

This interpretation is further supported by examining enriched categories of gene function within the set of differentially expressed genes. GO overrepresentation analysis showed that genes associated predominately with nervous system development, cell proliferation, neuron differentiation, lipid metabolism, RNA binding, and axon guidance were enriched in the set of downregulated genes (supplemental Table 1, available at www.jneurosci.org as supplemental material). Alternatively, upregulated genes showed enrichment for genes related to ion channel activity, voltage-gated ion channel activity, transporter activity, and glycoprotein metabolism. Thus, from P7 onward, there is a clear downregulation of early developmental functions and a shift toward the regulation of processes related to mature phenotype. Most prominent among these mature features are spiking behavior, which is conferred by the expression of ion channels, and increased energy metabolism, which is required to maintain ion homeostasis and sustain spiking activity.

Downregulated genes were not, however, restricted to those with overt developmental functions. GO overrepresentation analysis also revealed that ion channels, particularly sodium and calcium channels, were overrepresented in the set of downregulated genes. This is consistent with an emerging perspective on the development of excitable cells (Moody and Bosma, 2005), which emphasizes that the passage from immature to mature states cannot be understood as simply the progressive expression of a fixed "basis" set of ion channels that gradually accumulate to fill out the mature complement of expressed channels. Instead, subsets of ion channels often emerge and recede, reflecting the fact that specific ion channels support temporary developmental functions that are often essential to the induction of mature phenotype but are ultimately incompatible with the maintenance of that phenotype. Two recent studies have shown that embryonic day 13.5 freshly postmitotic interneurons express a variety of ion channels and synaptic-related genes (Batista-Brito et al., 2008; Marsh et al., 2008). Although some of these may persist throughout the life of these neurons, our data, which show that approximately equal numbers of ion channel and synapse-related genes are upregulated and downregulated postnatally, support the hypothesis that some of these early expressed channels and receptors may in fact serve transitory functions necessary for neuronal migration or for the differentiation of cell identity but may not directly contribute to the perseverance of the mature state.

These developmental changes in ion channel expression were reflected in changes in the electrophysiological properties of G42 cells. Over the first 4 postnatal weeks, G42 cells showed a sharp decline in input resistance, required greater current injection to reach spike threshold, integrated inputs over progressively smaller time windows, showed graded responses to a wider range of input currents, and achieved increasingly higher firing rates. Many of these changes characterized the maturation of other neuronal cell types (McCormick and Prince, 1987; Zhang, 2004; Plotkin et al., 2005; Doischer et al., 2008). Additionally, and con-

sistent with previous reports (Itami et al., 2007; Doischer et al., 2008), P7 and P10 G42 cells displayed spike-frequency adaptation, a feature lost by P15. Together, these data show that, as late as the beginning of the third postnatal week, G42 cells are electrophysiologically distinct from their mature phenotype, which develops gradually.

Some of the molecular mechanisms underlying the hallmarks of mature FS interneurons have been described. In particular, it is well appreciated that Kv3 potassium channels enable fast spiking in these cells by providing rapid membrane repolarization after an action potential (Erisir et al., 1999; Lau et al., 2000; Rudy and McBain, 2001). Our data corroborate this, showing a coincident increase in the maximum spike rate and the expression of the Kv3 potassium channel subunit encoding genes *Kcnc1* and *Kcnc2*. However, Kv3 channels alone do not necessarily fully account for fast spiking behavior, because they only mediate the falling phase of the action potential. Our data provide additional candidate genes that may also support this specialized function. *Scn8a* and *Scn4b* are two sodium channel subunit genes that are upregulated and are associated with the high-frequency repetitive spiking behavior of cerebellar Purkinje neurons (Grieco and Raman, 2004; Grieco et al., 2005; Levin et al., 2006). Additionally, the low input resistance and fast time constant observed in mature FS cells in part reflect upregulation of the two-pore potassium leak channels TWIK1 and TASK1, demonstrated by microarray, immunohistochemistry, and pharmacology. The increase in current threshold is also paralleled by the upregulation of several Shaker potassium channel subunits, *Kcna1*, *Kcna6*, *Kcnab1*, *Kcnab2*, and *Kcnab3*, that may dampen excitability.

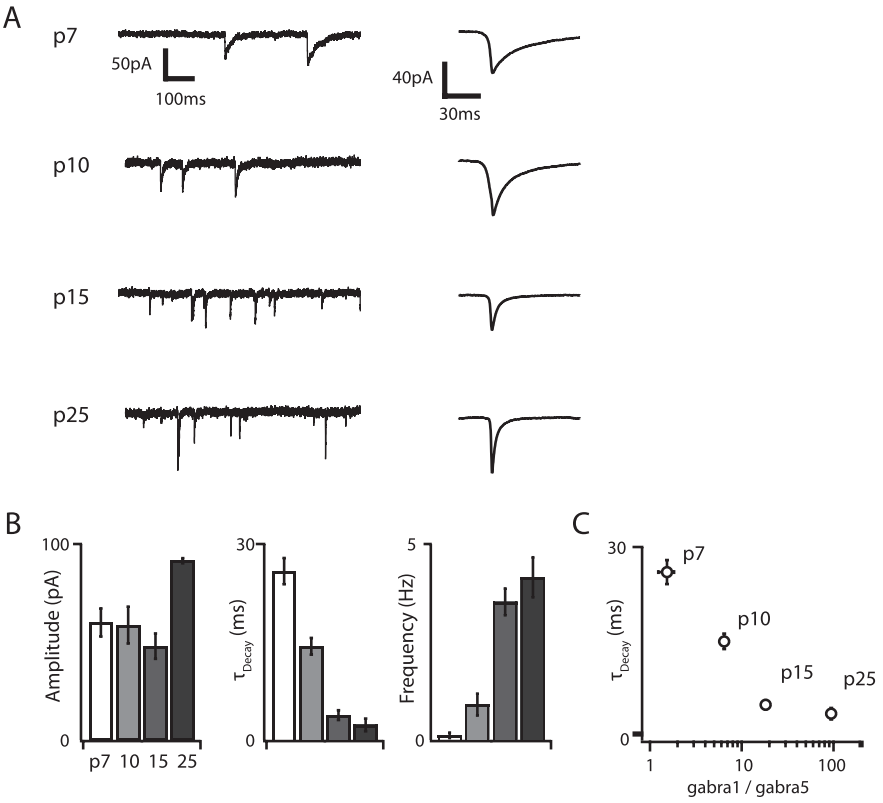

Figure 8. Inhibitory transmission is also strongly developmentally regulated in G42 FS interneurons. ***A***, Representative voltage traces recorded at V_{Hold} of −70 mV in the presence of glutamate receptor blockers, TTX, and with E_{Cl} of 0 mV at each developmental point (left traces) and corresponding average mIPSC waveforms (right traces). The developmental decrease in the mIPSC decay time constant is very apparent. ***B***, Population mIPSC amplitude, decay, and frequency averages over postnatal development. Unlike mEPSCs, maturational mIPSC changes are uniformly monotonic. ***C***, The mIPSC decay time constant is inversely correlated with age and with the log of the *gabra1/gabra5* ratio measured by microarray, suggesting that a $GABA_A$ receptor subunit switch is responsible for the striking decrease in mIPSC decay time constant over development. Error bars in ***C*** are propagated SEM.

In addition to observing dramatic changes in intrinsic physiology, we observed dynamic regulation of synaptic properties. We detected both mEPSCs and mIPSCs as early as P7, demonstrating that neocortical FS cells in somatosensory cortex receive functional inputs sometime before the close of the first postnatal week. The frequency and amplitude of mPSCs showed an overall increase between P7 and P25, consistent with this being a period of enhanced neocortical synaptogenesis. Although we did not directly explore mechanisms underlying this process, our microarray screen detected regulation of an assortment of cell adhesion molecules presumed to play a role in synaptic connectivity, such as *Ncam1*, *Ncam2*, *Clstn3*, *Farp2*, *Bcan*, *Hapln4*, *Hapln1*, *Vcan*, *Ncan*, Chl1, *Nxn1*, *Cxadr*, and *Fat4*. These present good candidates for future investigation of the regulation of cell-type-specific synaptic connectivity, particularly because some of these appear to be enriched or depleted in mature FS cells with respect to other cell types (Sugino et al., 2006).

Consistent with observed changes in mPSC amplitudes and kinetics, we observed regulation of multiple GABA and glutamate receptor subunits. *Gabra1* and *Gria4* show ~9-fold and 3-fold upregulation, respectively, whereas *Gabra5*, *Grik2*, and *Glra2* show 8-fold, 4-fold, and 14-fold downregulation. Although the increase in the ratio of *Gabra1* to *Gabra5* correlates with a developmental decrease in the decay time constant of mIPSCs in this and other cell types (Dunning et al., 1999), the functional implications of the regulation of these other receptors are not fully understood (Contractor et al., 2001; Ali, 2003; Braga et al., 2003, 2004; Fisahn et al., 2004; Young-Pearse et al., 2006).

Together, our intrinsic and synaptic results suggest that immature FS interneurons perform substantially different roles in cortical circuits than their mature counterparts. Narrow integration windows and high-frequency non-adapting firing allow mature FS cells to exert strong temporal control over the activity of their synaptic targets (Holmgren et al., 2003; Galarreta et al., 2004). Immature FS cells, however, have high input resistance, relatively long membrane time membrane constants, and exhibit spike-frequency adaptation. They therefore integrate input over broader temporal windows and transform that input with less temporal precision and presumably produce weaker inhibition than mature FS cells because of their lower firing rate. These features are poorly suited to mediate the timing and entrainment functions typically attributed to FS interneurons in mature cortical circuits (Doischer et al., 2008).

Conversely, the high input resistance and long integration window of immature FS cells may permit them to fire in response to the sparser and weaker synaptic inputs present as they begin to integrate into spontaneously active developing cortical circuits.

In many systems, spontaneous activity is transduced via Ca^{2+} influx into transcriptional changes required for normal maturation of intrinsic properties (Gu and Spitzer, 1995; Moody and Bosma, 2005; Spitzer, 2006) and circuit formation (Katz and Shatz, 1996). It is therefore tempting to speculate that enhanced expression of calcium channel subunits, especially *Cacna1g*, which mediates a low-threshold calcium current, as well as other channels that flux calcium are required early in development when synaptic input is minimal but that the need for these subunits is supplanted once synaptic inputs and firing patterns mature.

References

Ali AB (2003) Involvement of post-synaptic kainate receptors during synaptic transmission between unitary connections in rat neocortex. Eur J Neurosci 17:2344–2350.

Alifragis P, Liapi A, Parnavelas JG (2004) Lhx6 regulates the migration of cortical interneurons from the ventral telencephalon but does not specify their GABA phenotype. J Neurosci 24:5643–5648.

Bartos M, Vida I, Frotscher M, Meyer A, Monyer H, Geiger JR, Jonas P (2002) Fast synaptic inhibition promotes synchronized gamma oscillations in hippocampal interneuron networks. Proc Natl Acad Sci U S A 99:13222–13227.

Bartos M, Vida I, Jonas P (2007) Synaptic mechanisms of synchronized gamma oscillations in inhibitory interneuron networks. Nat Rev Neurosci 8:45–56.

Batista-Brito R, Machold R, Klein C, Fishell G (2008) Gene expression in cortical interneuron precursors is prescient of their mature function. Cereb Cortex 18:2306–2317.

Bond CT, Herson PS, Strassmaier T, Hammond R, Stackman R, Maylie J, Adelman JP (2004) Small conductance Ca^{2+}-activated K^+ channel knock-out mice reveal the identity of calcium-dependent afterhyperpolarization currents. J Neurosci 24:5301–5306.

Braga MF, Aroniadou-Anderjaska V, Xie J, Li H (2003) Bidirectional modulation of GABA release by presynaptic glutamate receptor 5 kainate receptors in the basolateral amygdala. J Neurosci 23:442–452.

Braga MF, Aroniadou-Anderjaska V, Li H (2004) The physiological role of kainate receptors in the amygdala. Mol Neurobiol 30:127–141.

Butt SJ, Fuccillo M, Nery S, Noctor S, Kriegstein A, Corbin JG, Fishell G (2005) The temporal and spatial origins of cortical interneurons predict their physiological subtype. Neuron 48:591–604.

Butt SJ, Cobos I, Golden J, Kessaris N, Pachnis V, Anderson S (2007) Transcriptional regulation of cortical interneuron development. J Neurosci 27:11847–11850.

Butt SJ, Sousa VH, Fuccillo MV, Hjerling-Leffler J, Miyoshi G, Kimura S, Fishell G (2008) The requirement of Nkx2–1 in the temporal specification of cortical interneuron subtypes. Neuron 59:722–732.

Cavallaro M, Mariani J, Lancini C, Latorre E, Caccia R, Gullo F, Valotta M, DeBiasi S, Spinardi L, Ronchi A, Wanke E, Brunelli S, Favaro R, Ottolenghi S, Nicolis SK (2008) Impaired generation of mature neurons by neural stem cells from hypomorphic Sox2 mutants. Development 135:541–557.

Chattopadhyaya B, Di Cristo G, Higashiyama H, Knott GW, Kuhlman SJ, Welker E, Huang ZJ (2004) Experience and activity-dependent maturation of perisomatic GABAergic innervation in primary visual cortex during a postnatal critical period. J Neurosci 24:9598–9611.

Cobb SR, Buhl EH, Halasy K, Paulsen O, Somogyi P (1995) Synchronization of neuronal activity in hippocampus by individual GABAergic interneurons. Nature 378:75–78.

Cobos I, Long JE, Thwin MT, Rubenstein JL (2006) Cellular patterns of transcription factor expression in developing cortical interneurons. Cereb Cortex 16 [Suppl 1]:i82–i88.

Colasante G, Collombat P, Raimondi V, Bonanomi D, Ferrai C, Maira M, Yoshikawa K, Mansouri A, Valtorta F, Rubenstein JL, Broccoli V (2008) Arx is a direct target of Dlx2 and thereby contributes to the tangential migration of GABAergic interneurons. J Neurosci 28:10674–10686.

Contractor A, Swanson G, Heinemann SF (2001) Kainate receptors are involved in short- and long-term plasticity at mossy fiber synapses in the hippocampus. Neuron 29:209–216.

Deepa SS, Carulli D, Galtrey C, Rhodes K, Fukuda J, Mikami T, Sugahara K, Fawcett JW (2006) Composition of perineuronal net extracellular matrix in rat brain: a different disaccharide composition for the net-associated proteoglycans. J Biol Chem 281:17789–17800.

Di Cristo G, Chattopadhyaya B, Kuhlman SJ, Fu Y, Bélanger MC, Wu CZ, Rutishauser U, Maffei L, Huang ZJ (2007) Activity-dependent PSA expression regulates inhibitory maturation and onset of critical period plasticity. Nat Neurosci 10:1569–1577.

Doischer D, Hosp JA, Yanagawa Y, Obata K, Jonas P, Vida I, Bartos M (2008) Postnatal differentiation of basket cells from slow to fast signaling devices. J Neurosci 28:12956–12968.

Du J, Zhang L, Weiser M, Rudy B, McBain CJ (1996) Developmental expression and functional characterization of the potassium-channel subunit Kv3.1b in parvalbumin-containing interneurons of the rat hippocampus. J Neurosci 16:506–518.

Dunning DD, Hoover CL, Soltesz I, Smith MA, O'Dowd DK (1999) GABA(A) receptor-mediated miniature postsynaptic currents and alpha-subunit expression in developing cortical neurons. J Neurophysiol 82:3286–3297.

Erisir A, Lau D, Rudy B, Leonard CS (1999) Function of specific K^+ channels in sustained high-frequency firing of fast-spiking neocortical interneurons. J Neurophysiol 82:2476–2489.

Fisahn A, Contractor A, Traub RD, Buhl EH, Heinemann SF, McBain CJ (2004) Distinct roles for the kainate receptor subunits GluR5 and GluR6 in kainate-induced hippocampal gamma oscillations. J Neurosci 24:9658–9668.

Flames N, Pla R, Gelman DM, Rubenstein JL, Puelles L, Marín O (2007) Delineation of multiple subpallial progenitor domains by the combinatorial expression of transcriptional codes. J Neurosci 27:9682–9695.

Flavell SW, Greenberg ME (2008) Signalling mechanisms linking neuronal activity to gene expression and plasticity of the nervous system. Annu Rev Neurosci 31:563–590.

Friocourt G, Kanatani S, Tabata H, Yozu M, Takahashi T, Antypa M, Raguénès O, Chelly J, Férec C, Nakajima K, Parnavelas JG (2008) Cell-autonomous roles of ARX in cell proliferation and neuronal migration during corticogenesis. J Neurosci 28:5794–5805.

Fulp CT, Cho G, Marsh ED, Nasrallah IM, Labosky PA, Golden JA (2008) Identification of Arx transcriptional targets in the developing basal forebrain. Hum Mol Genet 17:3740–3760.

Galarreta M, Erdélyi F, Szabó G, Hestrin S (2004) Electrical coupling among irregular-spiking GABAergic interneurons expressing cannabinoid receptors. J Neurosci 24:9770–9778.

Galtrey CM, Fawcett JW (2007) The role of chondroitin sulfate proteoglycans in regeneration and plasticity in the central nervous system. Brain Res Rev 54:1–18.

Grieco TM, Raman IM (2004) Production of resurgent current in $Na_V1.6$-null Purkinje neurons by slowing sodium channel inactivation with β-pompilidotoxin. J Neurosci 24:35–42.

Grieco TM, Malhotra JD, Chen C, Isom LL, Raman IM (2005) Open-channel block by the cytoplasmic tail of sodium channel beta4 as a mechanism for resurgent sodium current. Neuron 45:233–244.

Gu X, Spitzer NC (1995) Distinct aspects of neuronal differentiation encoded by frequency of spontaneous Ca^{2+} transients. Nature 375:784–787.

Guillemot F, Molnár Z, Tarabykin V, Stoykova A (2006) Molecular mechanisms of cortical differentiation. Eur J Neurosci 23:857–868.

Hamel MG, Ajmo JM, Leonardo CC, Zuo F, Sandy JD, Gottschall PE (2008) Multimodal signalling by the ADAMTSs (a disintegrin and metalloproteinase with thrombospondin motifs) promotes neurite extension. Exp Neurol 210:428–440.

Hempel CM, Sugino K, Nelson SB (2007) A manual method for the purification of fluorescently labeled neurons from the mammalian brain. Nat Protoc 2:2924–2929.

Hensch TK, Fagiolini M, Mataga N, Stryker MP, Baekkeskov S, Kash SF (1998) Local GABA circuit control of experience-dependent plasticity in developing visual cortex. Science 282:1504–1508.

Holmgren C, Harkany T, Svennenfors B, Zilberter Y (2003) Pyramidal cell communication within local networks in layer 2/3 of rat neocortex. J Physiol 551:139–153.

Iftinca MC, Zamponi GW (2009) Regulation of neuronal T-type calcium channels. Trends Pharmacol Sci 30:32–40.

Itami C, Kimura F, Nakamura S (2007) Brain-derived neurotrophic factor regulates the maturation of layer 4 fast-spiking cells after the second postnatal week in the developing barrel cortex. J Neurosci 27:2241–2252.

Katagiri H, Fagiolini M, Hensch TK (2007) Optimization of somatic inhibition at critical period onset in mouse visual cortex. Neuron 53:805–812.
Katz LC, Shatz CJ (1996) Synaptic activity and the construction of cortical circuits. Science 274:1133–1138.
Kawaguchi Y, Kondo S (2002) Parvalbumin, somatostatin and cholecystokinin as chemical markers for specific GABAergic interneuron types in the rat frontal cortex. J Neurocytol 31:277–287.
Kindler CH, Yost CS, Gray AT (1999) Local anesthetic inhibition of baseline potassium channels with two pore domains in tandem. Anesthesiology 90:1092–1102.
Kong JH, Adelman JP, Fuchs PA (2008) Expression of the SK2 calcium-activated potassium channel is required for cholinergic function in mouse cochlear hair cells. J Physiol 586:5471–5485.
Lau D, Vega-Saenz de Miera EC, Contreras D, Ozaita A, Harvey M, Chow A, Noebels JL, Paylor R, Morgan JI, Leonard CS, Rudy B (2000) Impaired fast-spiking, suppressed cortical inhibition, and increased susceptibility to seizures in mice lacking Kv3.2 K^+ channel proteins. J Neurosci 20:9071–9085.
Le Roux N, Amar M, Moreau A, Baux G, Fossier P (2008) Impaired GABAergic transmission disrupts normal homeostatic plasticity in rat cortical networks. Eur J Neurosci 27:3244–3256.
Lesage F, Lazdunski M (2000) Molecular and functional properties of two-pore-domain potassium channels. Am J Physiol Renal Physiol 279:F793–F801.
Levin SI, Khaliq ZM, Aman TK, Grieco TM, Kearney JA, Raman IM, Meisler MH (2006) Impaired motor function in mice with cell-specific knockout of sodium channel Scn8a (NaV1.6) in cerebellar purkinje neurons and granule cells. J Neurophysiol 96:785–793.
Lieuw KH, Li G, Zhou Y, Grosveld F, Engel JD (1997) Temporal and spatial control of murine GATA-3 transcription by promoter-proximal regulatory elements. Dev Biol 188:1–16.
Liodis P, Denaxa M, Grigoriou M, Akufo-Addo C, Yanagawa Y, Pachnis V (2007) Lhx6 activity is required for the normal migration and specification of cortical interneuron subtypes. J Neurosci 27:3078–3089.
Liu X, Herbison AE (2008) Small-conductance calcium-activated potassium channels control excitability and firing dynamics in gonadotropin-releasing hormone (GnRH) neurons. Endocrinology 149:3598–3604.
Lyckman AW, Horng S, Leamey CA, Tropea D, Watakabe A, Van Wart A, McCurry C, Yamamori T, Sur M (2008) Gene expression patterns in visual cortex during the critical period: synaptic stabilization and reversal by visual deprivation. Proc Natl Acad Sci U S A 105:9409–9414.
Maravall M, Stern EA, Svoboda K (2004) Development of intrinsic properties and excitability of layer 2/3 pyramidal neurons during a critical period for sensory maps in rat barrel cortex. J Neurophysiol 92:144–156.
Markram H, Toledo-Rodriguez M, Wang Y, Gupta A, Silberberg G, Wu C (2004) Interneurons of the neocortical inhibitory system. Nat Rev Neurosci 5:793–807.
Marsh ED, Minarcik J, Campbell K, Brooks-Kayal AR, Golden JA (2008) FACS-array gene expression analysis during early development of mouse telencephalic interneurons. Dev Neurobiol 68:434–445.
McCormick DA, Prince DA (1987) Post-natal development of electrophysiological properties of rat cerebral cortical pyramidal neurones. J Physiol 393:743–762.
McCormick DA, Connors BW, Lighthall JW, Prince DA (1985) Comparative electrophysiology of pyramidal and sparsely spiny stellate neurons of the neocortex. J Neurophysiol 54:782–806.
McRae PA, Rocco MM, Kelly G, Brumberg JC, Matthews RT (2007) Sensory deprivation alters aggrecan and perineuronal net expression in the mouse barrel cortex. J Neurosci 27:5405–5413.
Moody WJ, Bosma MM (2005) Ion channel development, spontaneous activity, and activity-dependent development in nerve and muscle cells. Physiol Rev 85:883–941.
Nelson SB, Sugino K, Hempel CM (2006) The problem of neuronal cell types: a physiological genomics approach. Trends Neurosci 29:339–345.
Plotkin JL, Wu N, Chesselet MF, Levine MS (2005) Functional and molecular development of striatal fast-spiking GABAergic interneurons and their cortical inputs. Eur J Neurosci 22:1097–1108.
Rudy B, McBain CJ (2001) Kv3 channels: voltage-gated K+ channels designed for high-frequency repetitive firing. Trends Neurosci 24:517–526.
Semeralul MO, Boutros PC, Likhodi O, Okey AB, Van Tol HH, Wong AH (2006) Microarray analysis of the developing cortex. J Neurobiol 66:1646–1658.
Shirasaki R, Pfaff SL (2002) Transcriptional codes and the control of neuronal identity. Annu Rev Neurosci 25:251–281.
Spitzer NC (2006) Electrical activity in early neuronal development. Nature 444:707–712.
Stead JD, Neal C, Meng F, Wang Y, Evans S, Vazquez DM, Watson SJ, Akil H (2006) Transcriptional profiling of the developing rat brain reveals that the most dramatic regional differentiation in gene expression occurs postpartum. J Neurosci 26:345–353.
Sugino K, Hempel CM, Miller MN, Hattox AM, Shapiro P, Wu C, Huang ZJ, Nelson SB (2006) Molecular taxonomy of major neuronal classes in the adult mouse forebrain. Nat Neurosci 9:99–107.
Sussel L, Marin O, Kimura S, Rubenstein JL (1999) Loss of Nkx2.1 gene function results in ventral to dorsal molecular respecification within the basal telencephalon: evidence for a transformation of the pallidum into the striatum. Development 126:3359–3370.
Torborg CL, Berg AP, Jeffries BW, Bayliss DA, McBain CJ (2006) TASK-like conductances are present within hippocampal CA1 stratum oriens interneuron subpopulations. J Neurosci 26:7362–7367.
Treiman DM (2001) GABAergic mechanisms in epilepsy. Epilepsia 42 [Suppl 3]:8–12.
Wang DD, Kriegstein AR (2008) GABA regulates excitatory synapse formation in the neocortex via NMDA receptor activation. J Neurosci 28:5547–5558.
Wonders CP, Anderson SA (2006) The origin and specification of cortical interneurons. Nat Rev Neurosci 7:687–696.
Xu Q, Tam M, Anderson SA (2008) Fate mapping Nkx2.1-lineage cells in the mouse telencephalon. J Comp Neurol 506:16–29.
Xu Q, Cobos I, De La Cruz E, Rubenstein JL, Anderson SA (2004) Origins of cortical interneuron subtypes. J Neurosci 24:2612–2622.
Young-Pearse TL, Ivic L, Kriegstein AR, Cepko CL (2006) Characterization of mice with targeted deletion of glycine receptor alpha 2. Mol Cell Biol 26:5728–5734.
Zhang ZW (2004) Maturation of layer V pyramidal neurons in the rat prefrontal cortex: intrinsic properties and synaptic function. J Neurophysiol 91:1171–1182.
Zhao Y, Flandin P, Long JE, Cuesta MD, Westphal H, Rubenstein JL (2008) Distinct molecular pathways for development of telencephalic interneuron subtypes revealed through analysis of Lhx6 mutants. J Comp Neurol 510:79–99.